metals

MDPI

Article

Volatile Resistive Switching Characteristics of $Pt/HfO_2/TaO_x/TiN$ Short-Term Memory Device

Hojeong Ryu and Sungjun Kim *

Division of Electronics and Electrical Engineering, Dongguk University, Seoul 04620, Korea; hojeong.ryu95@gmail.com
* Correspondence: sungjun@dongguk.edu

Abstract: In this work, we study the threshold switching and short-term memory plasticity of a $Pt/HfO_2/TaO_x/TiN$ resistive memory device for a neuromorphic system. First, we verify the thickness and elemental characterization of the device stack through transmission electron microscopy (TEM) and an energy-dispersive X-ray spectroscopy (EDS) line scan. Volatile resistive switching with low compliance current is observed under the DC sweep in a positive bias. Uniform cell-to-cell and cycle-to-cycle DC I-V curves are achieved by means of a repetitive sweep. The mechanism of volatile switching is explained by the temporal generation of traps. Next, we initiate the accumulation of the conductance and a natural decrease in the current by controlling the interval time of the pulses. Finally, we conduct a neuromorphic simulation to calculate the pattern recognition accuracy. These results can be applicable to short-term memory applications such as temporal learning in a neuromorphic system.

Keywords: resistive switching; synaptic device; short-term memory; threshold switching

Citation: Ryu, H.; Kim, S. Volatile Resistive Switching Characteristics of $Pt/HfO_2/TaO_x/TiN$ Short-Term Memory Device. *Metals* **2021**, *11*, 1207. https://doi.org/10.3390/met11081207

Academic Editor: Lijun Zhang

Received: 12 July 2021
Accepted: 25 July 2021
Published: 29 July 2021

1. Introduction

Resistive-switching behaviors that are observed, including resistive switching random-access memory (RRAM) [1], phase-change random-access memory (PRAM) [2], and magnetic random-access memory (MRAM) [3], can be an important phenomenon in non-volatile memory applications. The resistive switching of PRAM occurs through a TiN heater in which two states are reversible by a melting and quenching operation. MRAM uses a magnetic storage element for resistive switching. One ferromagnetic plate is the reference layer and the magnetization alignment of the other layer can be changed by the electric field.

Bipolar resistive switching provides metal oxide-based RRAM devices with competitive performance due to their fast operation speed, low switching voltage, low current level, multi-level cells (MLC) capability, and CMOS compatibility [4–17]. Resistive change switching of RRAM can be expanded in more directions depending on the type and operation method of the device stack. For example, a self-rectification phenomenon is observed in the case of a stack with two layers of insulators, and there is a large difference in work functions between the top and bottom electrodes [18]. In addition, the type of switching can vary depending on whether or not electroforming is performed, as well as the limitation of the operating current [18]. For example, a high current (milliampere) shows a strong non-volatile characteristic while a low current (microampere or less) shows a more volatile characteristic. However, most previous papers have demonstrated current reduction (reset process) through the opposite sweep of the set process without strictly checking whether it is non-volatile or volatile at low currents [19,20].

Recently, the existing von Neumann structure has been shown to have disadvantages, such as a bottleneck between memory and process. A neuromorphic system that emulates the concept of biological neuron and synapse is emerging that allows for the efficient processing of large amounts of data in the era of big data [21]. The cross-point array

including RRAM cells can act as an artificial synapse in a neuromorphic system by using vector-matrix multiplication. The requirements of RRAM as an artificial synapse include MLC, high endurance, good variability, and low energy consumption [22]. The short-term memory effect of the memristor can provide temporal information processing, which is suitable for reservoir computing applications [23–25].

In this work, we fabricated a Pt/HfO_2/TiO_x/TiN RRAM device with self-rectification, and we characterized the electrical measurement for short-term memory. First, the self-rectification characteristics are explained by the conduction model. The short-term plasticity was characterized by pulse operations after confirmation of the cell-to-cell and cycle-to-cycle DC sweep. Finally, the pattern recognition rate was calculated through neuromorphic simulation.

2. Materials and Methods

The RRAM devices were prepared as follows. A-100-nm thick TiN bottom electrode was deposited by DC sputtering on SiO_2/Si substrate. Next, 20 nm thick TaO_x was deposited sequentially via pulsed DC reactive sputtering on the TiN layer. The gas flow rates of Ar and O_2 were 8 sccm and 12 sccm, respectively, with the base pressure of 1.6×10^{-6} Torr and the deposition pressure of 1 mTorr. A 7 nm thick HfO_2 layer was deposited by the atomic layer deposition (ALD) technique on the TaO_x layer. The HfO_2 film was deposited using TEMAHf and H_2O at an internal temperature of 280 °C using a thermal and plasma-enhanced ALD process (CN1, Atomic premium). Finally, a-100-nm thick Pt was deposited as the top electrode using e-beam evaporation (FR-EB20, ULTEC, Daegu, Korea) on the TaO_x layer, and the Pt top electrode patterning was conducted via a shadow mask including circular patterns with 100 μm. The cross-section of the Pt/HfO_2/TaO_x/TiN device was observed using transmission electron microscopy (TEM) (JEOL/CEOS, JEM-2100F, Cs corrector, Tokyo, Japan) and energy-dispersive X-ray spectroscopy (EDS). The current–voltage (I-V) curves and transient curves of the RRAM cells were measured using a semiconductor parameter analyzer (Keithley 4200-SCS and 4225-PMU ultrafast module, Cleveland, OH, USA) while a bias was applied to the Pt top electrode and the TiN bottom electrode was grounded. The accuracy of the current level was measured to be 100 pA.

3. Results and Discussion

Figure 1a,b shows a scanning transmission electron microscopy (STEM) image and EDS line scan of the Pt/HfO_2/TaO_x/TiN device. The two insulators (HfO_2 and TaO_x) can be distinguished through the contrast in STEM values, as shown in Figure 1a. Figure 1b shows Wt (%) as a function of the distance obtained by EDS line scan for Hf, Ta, Pt, N, O, and Ti. Figure 1c shows a high-resolution TEM image of the Pt/HfO_2/TaO_x/TiN device. The thicknesses of HfO_2 and TaO_x are about 7 nm and 20 nm. The polycrystalline TiN layer and the amorphous HfO_2 and TaO_x layers can be clearly observed in the TEM image.

Next, we measured the I-V curves of the Pt/HfO_2/TaO_x/TiN device to confirm the volatile memory characteristics. Figure 2a,b, respectively, show the I-V curves for 10 cycles in one device and the first curve of 10 cells. It should be noted that a forming-less curve is observed with a compliance current of 100 nA in which the first curve and the subsequent curves are similar to each other. During dual DC sweep mode, the return curve current is higher than the forward current, and under the same conditions, the current of the subsequent DC sweep follows the initial current again. This indicates that the device has a volatile property. In other words, a temporarily increased current has a short-term memory effect that does not maintain that state. As a result, it is found that it is pointless to sweep with negative bias to reset. However, a similar curve is not observed at negative bias (not shown here) due to the rectification property of the Pt/HfO_2/TaO_x/TiN device in the forming-less mode. The rectifying behavior occurs due to the asymmetric work function of the top and bottom electrode without the forming process.

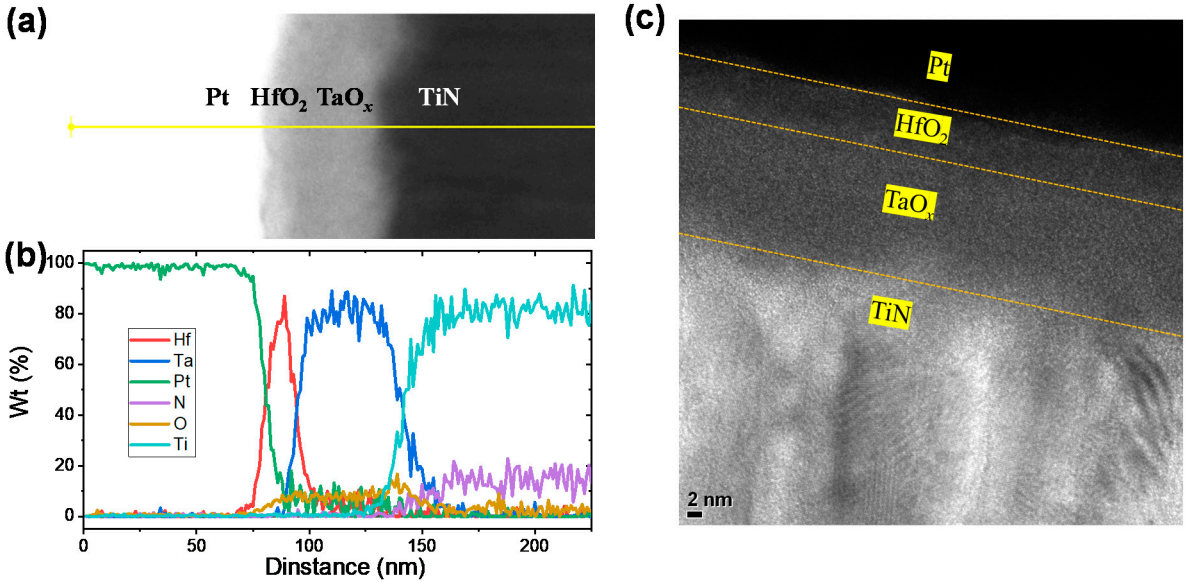

Figure 1. (**a**) STEM image, (**b**) EDS line scan, and (**c**) TEM image of $Pt/HfO_2/TaO_x/TiN$ RRAM device.

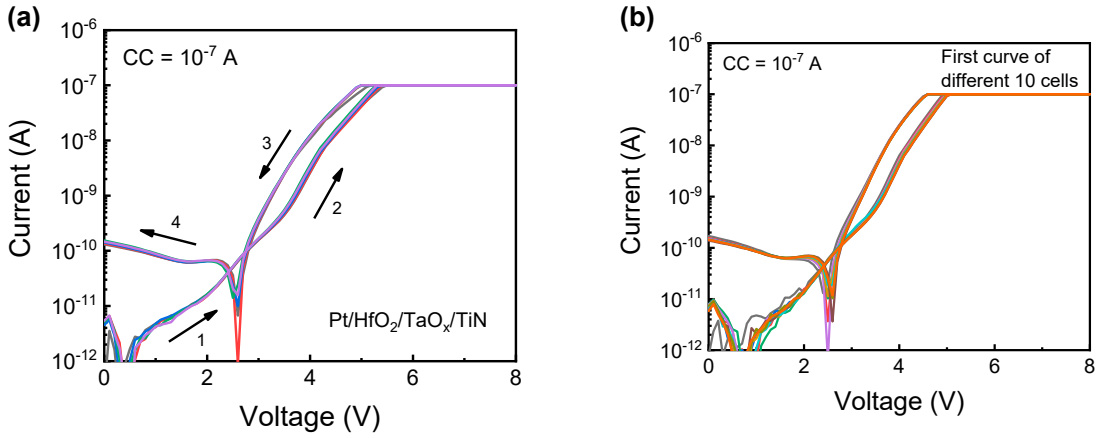

Figure 2. I–V characteristics of $Pt/HfO_2/TaO_x/TiN$ RRAM device. (**a**) Ten cycles in one cell and (**b**) first curves of 10 cells.

For the initial current level, the currents of less than about 100 pA are not accurate due to the range of detection of the current accuracy of the measuring equipment.

The possible volatile switching mechanism of short-term memory can be explained through the interface type model considering the presence of no electroforming and a progressively increasing current [26]. The HfO_2 layer is known as the main switching layer in the $Pt/HfO_2/TaO_x/TiN$ device [27]. Due to the current limitation caused by very low compliance, the filament production (the creation of oxygen vacancies in insulators) is limited, which leads to a temporary increase in current, but the filament understandably breaks down again in a short time. The volatile resistive switching behaviors were reported in different types, such as conductive bridge random-access memory (CBRAM) [28] and different metal oxide systems [29,30].

Next, we conduct pulse measurements to obtain the short-term memory characteristics for practical device operation. The natural reduction in current is important in short-term memory. The pulse inputs are designed by controlling the pulse interval time between pulses to observe the current accumulation and decay, as shown in Figure 3. For the accumulation curve, a strong signal input should be provided, and this is also the case for the decay curve. On the other hand, a weak signal input should be entered into the device. To begin, 60 pulses with a voltage of 9.5 V were applied at an interval of 0.001 s. In this short interval time condition, the current is gradually accumulated. The increase in current

can be clearly identified through the magnification of 16 pulses. However, the increased current is decayed when increasing the interval from 0.01 s to 0.055 s. Finally, the state of the device returns to its initial state, thus showing the short-term memory effect. These results indicate that even if pulses of the same voltage are applied, how frequently they are applied can further determine the conductance accumulation and attenuation. In other words, the dynamics of increasing of oxygen vacancies by pulse and the natural decrease in oxygen vacancies can be controlled.

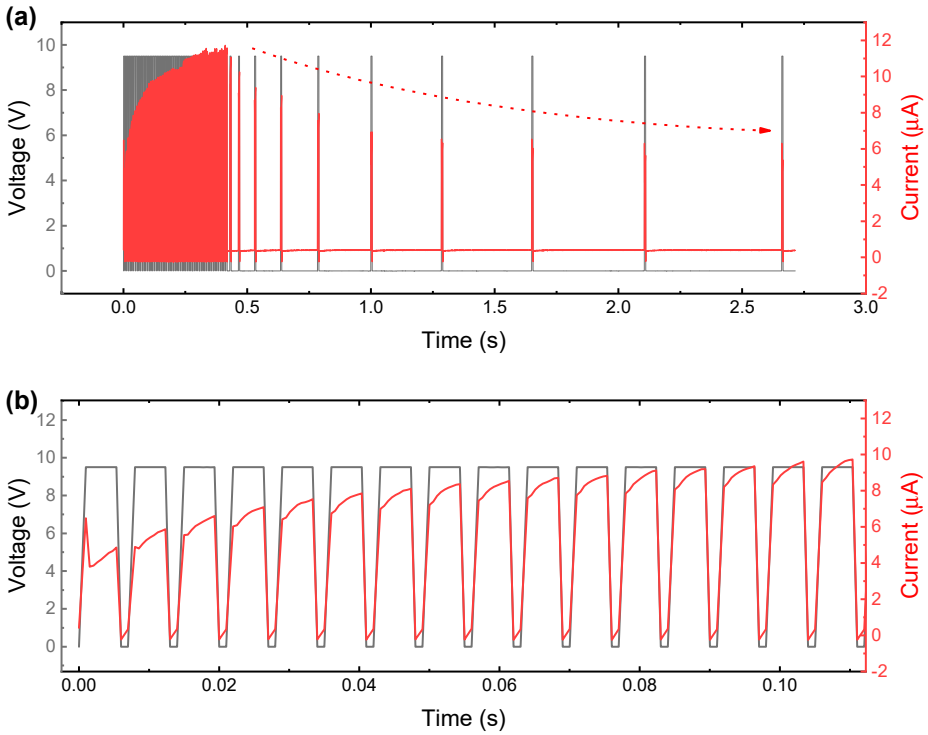

Figure 3. (**a**) Accumulation and decay characteristics of Pt/HfO_2/TaO_x/TiN RRAM device by pulse inputs. (**b**) Initial 15 pulses with progressively increasing current.

Next, we measured the cycle-to-cycle and cell-to-cell variation of the Pt/HfO_2/TaO_x/TiN device. Each of 10 cycles from 10 cells was continuously measured by applying the method illustrated in Figure 3. Figure 4a,b show the accumulation and decay curves of 10 cycles and their change rate between the initial current and final current, respectively. The rate of change is defined as follows:

$$Rate\ of\ change = \frac{final\ current - initial\ current}{initial\ current} \times 100\ (\%).$$

The rate of change should be small to reduce variability in the iterative accumulation and decay process. A change of 3% or less was observed in all 10 cycles. Figure 4c,d show the accumulation and decay curves of the first cycle of 10 cells and their change rate. The change rate of the first cycle is 3% or more. Figures S1 and S2 show the 10 cycles of the 10 cells.

Finally, we perform pattern recognition accuracy of Fashion MNIST by constructing a 3-layer neural network (784 × 128 × 10) when applying the conductance update of the Pt/HfO_2/TaO_x/TiN device in Figure 5a [31]. To classify the pattern images of the Fashion MNIST dataset, a 28 × 28 pixels image is normalized with a value between 0 and 1, and the images are unfolded to a 1-dimensional array (784 × 1) for the number of input neurons. The neural network has 128 nodes for the hidden layer. Each output node corresponds to the 10 classes of training and test images which correspond to the 10 output nodes. All neuron nodes in the neural network are fully connected with an imaginary artificial

synaptic array ($Pt/HfO_2/TaO_x/TiN$ device array) in which the weight has a quantized value, and a cross-point array structure can be performed by a vector-matrix multiplication operation. Figure 5b shows the result of the accuracy test as a function of epoch, in which the maximum accuracy is 88.6%.

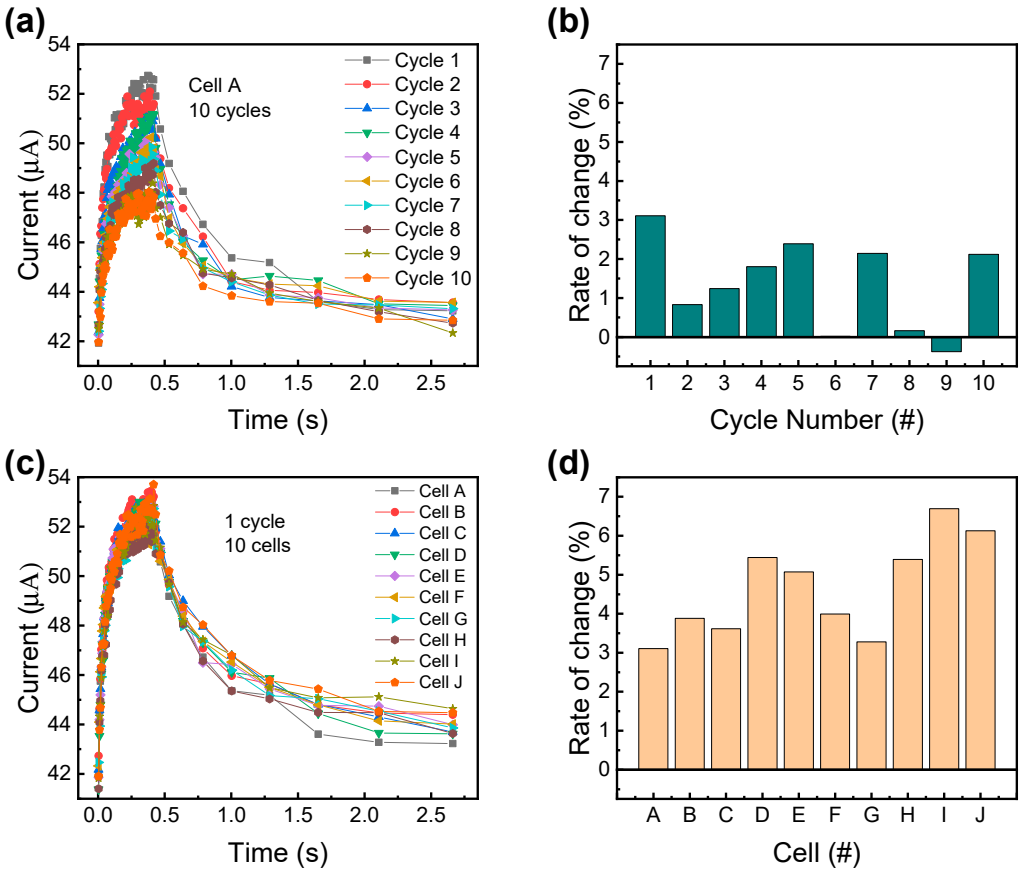

Figure 4. Accumulation and decay curves of the $Pt/HfO_2/TaO_x/TiN$ RRAM device. (**a**) Cycle-to-cycle variation and (**b**) their change rate. (**c**) Cell-to-cell variation and (**d**) their change rate.

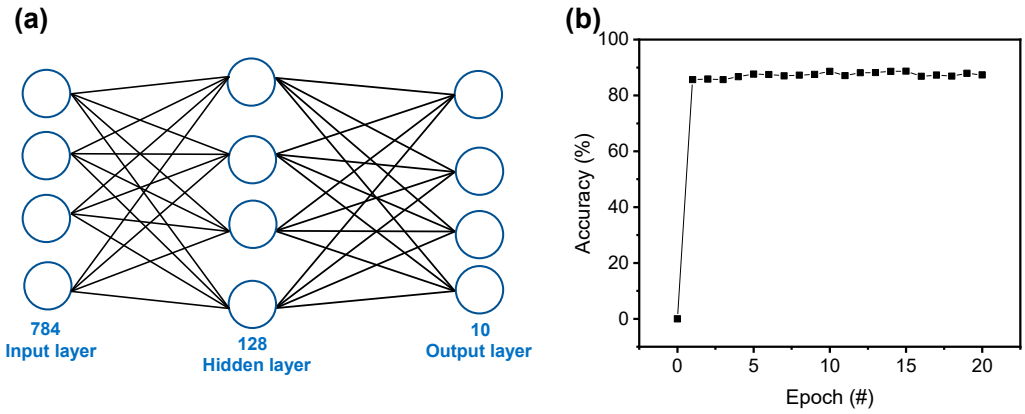

Figure 5. (**a**) Neural network including the input layer, hidden layer, and output layer. (**b**) Pattern recognition accuracy.

4. Conclusions

This study investigates the volatile resistive switching with the short-term memory effect of a $Pt/HfO_2/TaO_x/TiN$ resistive memory device. First, the thickness and material characterization of the device stack were confirmed by means of a TEM image, as well as STEM and an EDS line scan. The volatile resistive switching is secured, which adequately

conducts the DC sweep with low compliance current (100 nA). The variability (<7%) of the cell-to-cell and cycle-to-cycle DC I-V curves are obtained through the DC sweep curves. The accumulation and decay of the conductance are well controlled by the low frequency and high frequency of the pulse, respectively. Finally, neural network simulation is performed to test the pattern recognition accuracy. These results can be used to aid temporal learning in neuromorphic systems.

Supplementary Materials: The following are available online at https://www.mdpi.com/article/10.3390/met11081207/s1, Figure S1: 10 cycles of 10 cells for current decay, Figure S2: Change of rate for 10 cycles of 10 cells.

Author Contributions: H.R. conducted the electrical measurements and wrote the manuscript. S.K. conceptualized the experiment and supervised the study. Both authors have read and agreed to the published version of the manuscript.

Funding: This work was supported by the Korea Institute of Energy Technology Evaluation and Planning (KETEP) and the Ministry of Trade, Industry & Energy (MOTIE) of the Republic of Korea (no.20194030202320) and by a National Research Foundation of Korea (NRF) grant funded by Ministry of Science and ICT (2021R1C1C1004422).

Institutional Review Board Statement: Not applicable.

Informed Consent Statement: Not applicable.

Data Availability Statement: Not applicable.

Conflicts of Interest: The authors declare no conflict of interest.

References

1. Waser, R.; Dittmann, R.; Staikov, G.; Szot, K. Redox-Based Resistive Switching Memories—Nanoionic Mechanisms, Prospects, and Challenges. *Adv. Mater.* **2009**, *21*, 2632–2663. [CrossRef]
2. Fong, S.W.; Neumann, C.M.; Wong, H.S.P. Phase-Change Memory—Towards a Storage-Class Memory. *IEEE Trans. Electron. Mater.* **2017**, *64*, 4374–4385. [CrossRef]
3. Zhao, W.S.; Zhang, Y.; Devolder, Y.; Klein, J.O.; Ravelosona, D.; Chappert, C.; Mazoyer, P. Failure and reliability analysis of STT-MRAM. *Microelectron. Rel.* **2012**, *52*, 1848–1852. [CrossRef]
4. Lee, M.J.; Lee, C.B.; Lee, D.; Lee, S.R.; Chang, M.; Hur, J.H.; Kim, Y.B.; Kim, C.J.; Seo, D.H.; Seo, S.; et al. A fast, high endurance and scalable non-volatile memory device made from asymmetric Ta_2O_{5-x}/TaO_{2-x} bilayer structures. *Nat. Mat.* **2011**, *10*, 625–630. [CrossRef]
5. Wu, M.C.; Lin, Y.-W.; Jang, W.-Y.; Lin, C.-H.; Tseng, T.-Y. Low-power and highly reliable multilevel operation in ZrO_2 1T1R RRAM. *IEEE Electron. Device Lett.* **2011**, *32*, 1026–1028. [CrossRef]
6. Wang, Y.; Liu, Q.; Long, S.; Wang, W.; Wang, Q.; Zhang, M.; Zhang, S.; Li, Y.; Zuo, Q.; Yang, J.; et al. Investigation of resistive switching in Cu-doped HfO_2 thin film for multilevel non-volatile memory applications. *Nanotechnology* **2010**, *21*, 045202. [CrossRef]
7. Ryu, H.; Choi, J.; Kim, S. Voltage Amplitude-Controlled Synaptic Plasticity from Complementary Resistive Switching in Alloying HfO_x with AlO_x-Based RRAM. *Metals* **2020**, *10*, 1410. [CrossRef]
8. Su, T.-H.; Lee, K.-J.; Wang, L.-W.; Chang, Y.-C.; Wang, Y.-H. Resistive Switching Behavior of Magnesium Zirconia Nickel Nanorods. *Materials* **2020**, *13*, 2755. [CrossRef]
9. Yang, J.; Ryu, H.; Kim, S. Resistive and synaptic properties modulation by electroforming polarity in CMOS-compatible $Cu/HfO_2/Si$ device. *Chaos Solitons Fractals* **2021**, *145*, 110783. [CrossRef]
10. Mahata, C.; Kim, S. Modified resistive switching performance by increasing Al concentration in HfO2 on transparent indium tin oxide electrode. *Ceram. Inter.* **2021**, *47*, 1199–1207. [CrossRef]
11. Ryu, H.; Kim, S. Irregular Resistive Switching Behaviors of Al_2O_3-Based Resistor with Cu Electrode. *Metals* **2021**, *11*, 653. [CrossRef]
12. Chand, U.; Huang, K.C.; Huang, C.Y.; Tseng, T.Y. Mechanism of nonlinear switching in HfO_2-based crossbar RRAM with inserting large bandgap tunneling barrier layer. *IEEE Trans. Electron. Dev.* **2015**, *62*, 3665–3670. [CrossRef]
13. Ryu, H.; Kim, S. Gradually Tunable Conductance in TiO_2/Al_2O_3 Bilayer Resistors for Synaptic Device. *Metals* **2021**, *11*, 440. [CrossRef]
14. Zhang, Z.; Wang, F.; Hu, K.; She, Y.; Song, S.; Song, Z.; Zhang, K. Improvement of Resistive Switching Performance in Sulfur-Doped HfOx-Based RRAM. *Materials* **2021**, *14*, 3330. [CrossRef]
15. Yen, T.-J.; Chin, A.; Gritsenko, V. Improved Device Distribution in High-Performance SiNx Resistive Random Access Memory via Arsenic Ion Implantation. *Nanomaterials* **2021**, *11*, 1401. [CrossRef]

16. Simanjuntak, F.M.; Ohno, T.; Chandrasekaran, S.; Tseng, T.Y.; Samukawa, S. Neutral oxygen irradiation enhanced forming-less ZnO-based transparent analog memristor devices for neuromorphic computing applications. *Nanotechnology* **2020**, *31*, 26LT01. [CrossRef]
17. Chang, L.Y.; Simanjuntak, F.M.; Hsu, C.L.; Chandrasekaran, S.; Tseng, T.Y. Suboxide interface induced digital-to-analog switching transformation in all Ti-based memristor devices. *Appl. Phys. Lett.* **2020**, *117*, 073504. [CrossRef]
18. Ryu, H.; Kim, S. Self-Rectifying Resistive Switching and Short-Term Memory Characteristics in Pt/HfO_2/TaOx/TiN Artificial Synaptic Device. *Nanomaterial* **2020**, *10*, 2159. [CrossRef]
19. Park, J.H.; Jeon, D.S.; Kim, T.G. Ti-doped GaOx Resistive Switching Memory with Self-rectifying Behavior by using NbOx/Pt Bilayers. *ACS Appl. Mater. Interfaces* **2017**, *9*, 43336–43342. [CrossRef]
20. Wang, W.; Wang, R.; Shi, T.; Wie, J.; Cao, R.; Zhao, X.; Wu, Z.; Zhang, X.; Lu, J.; Xi, H.; et al. A Self-Rectification and Quasi-Linear Analogue Memristor for Artificial Neural Networks. *IEEE Electron Device Lett.* **2019**, *40*, 1407–1410. [CrossRef]
21. Yang, J.J.; Strukov, D.B.; Stewart, D.R. Memristive devices for computing. *Nat. Nanotechnol.* **2013**, *8*, 13–24. [CrossRef]
22. Zhu, J.; Zhang, T.; Yang, Y.; Huang, R. A comprehensive review on emerging artificial neuromorphic devices. *Appl. Phys. Rev.* **2020**, *7*, 011312. [CrossRef]
23. Zhong, Y.; Tang, J.; Li, X.; Gao, B.; Qian, H.; Wu, H. Dynamic memristor-based reservoir computing for high-efficiency temporal signal processing. *Nat. Commun.* **2021**, *12*, 408. [CrossRef]
24. Du, C.; Cai, F.; Zidan, M.A.; Ma, W.; Lee, S.H.; Lu, W.D. Reservoir computing using dynamic memristors for temporal information processing. *Nat. Commun.* **2017**, *8*, 2204. [CrossRef] [PubMed]
25. Yang, J.; Cho, H.; Ryu, H.; Ismail, M.; Mahata, C.; Kim, S. Tunable Synaptic Characteristics of a Ti/TiO_2/Si Memory Device for Reservoir Computing. *ACS Appl. Mater. Interfaces* **2021**, *13*, 33244–33252. [CrossRef] [PubMed]
26. Sawa, A. Resistive switching in transition metal oxides. *Mater. Today* **2008**, *11*, 28–36. [CrossRef]
27. Yoon, J.H.; Song, S.J.; Yoo, I.H.; Seok, J.Y.; Yoon, K.J.; Kwon, D.E.; Park, T.H.; Hwang, C.S. Highly Uniform, Electroforming-Free, and Self-Rectifying Resistive Memory in the Pt/Ta_2O_5/HfO_2-x/TiN Structure. *Adv. Funct. Mater.* **2014**, *24*, 5086–5095. [CrossRef]
28. Wang, W.; Wang, M.; Ambrosi, E.; Bricalli, A.; LAudato, M.; Sun, Z.; Chen, X.; Ielmini, D. Surface diffusion-limited lifetime of silver and copper nanofilaments in resistive switching devices. *Nat. Commun.* **2019**, *10*, 81. [CrossRef] [PubMed]
29. Cho, H.; Kim, S. Enhancing Short-Term Plasticity by Inserting a Thin TiO_2 Layer in WOx-Based Resistive Switching Memory. *Coatings* **2020**, *10*, 908. [CrossRef]
30. Cho, H.; Kim, S. Short-Term Memory Dynamics of TiN/Ti/TiO2/SiOx/Si Resistive Random Access Memory. *Nanomaterials* **2020**, *10*, 1821. [CrossRef]
31. Rahmani, M.K.; Kim, M.-H.; Hussain, F.; Abbas, Y.; Ismail, M.; Hong, K.; Mahata, C.; Choi, C.; Park, B.-G.; Kim, S. Memristive and Synaptic Characteristics of Nitride-Based Heterostructures on Si Substrate. *Nanomaterials* **2020**, *10*, 994. [CrossRef] [PubMed]